Xu, J.; Koldunov, N.; Remedio, A.; Sein, D.; Rechid, D.; Zhi, X.; Jiang, X.; Xu, M.; Zhu, X.; Fraedrich, K.; Jacob, D.:

Downstream effect of Hengduan Mountains on East China in the REMO regional climate model.

In: Theoretical and Applied Climatology. Vol. 135 (2019) 3 - 4, 1641 - 1658.

First published online by Springer: 14.12.2018

https://dx.doi.org/10.1007/s00704-018-2721-0

Downstream effect of Hengduan Mountains on East China in the REMO regional climate model

Jingwei Xu [1,2,3] & Nikolay V. Koldunov [4,5] & Armelle Reca C. Remedio [2] & Dmitry V. Sein [5,6] & Diana Rechid [2] & Xiefei Zhi [1] & Xi Jiang [1] & Min Xu [7] & Xiuhua Zhu [8] & Klaus Fraedrich [1,3] & Daniela Jacob [2]

Abstract
The Hengduan Mountains and Tibetan Plateau possess unique topographical characteristics that serve as an effective blocking of the movement of the westerly wind in the middle and lower troposphere towards East China. This study examines results from a regional climate model (REMO) at the resolutions of 25 and 50 km for the period 1980–2012. The model is run using lateral boundary conditions from ERA-Interim (European Centre for Medium-Range Weather Forecasts interim reanalysis). There are only a few differences between 25 and 50 km in land surface/vegetation characteristics, but the major differences in this region are due to the orography. Results show that the high-resolution simulation performance is poor in winter, when southwesterly wind prevails, whereas it performs well in summer, when the westerly wind is substantially weakened in southern China. In comparison to the ERA-Interim wind field, the high-resolution simulation overestimates the air flow over the Hengduan Mountains near the ground surface, which influences the transport of atmospheric water vapor in the downstream region, i.e., over southern China. Specifically, with the help of the overestimated southwesterly wind, the amount of atmospheric water vapor transported increases considerably perennially by up to 20% in southern China, while it decreases remarkably by more than 5%throughout the year in a large area of Central and North China. These features lead to excessive precipitation and underestimated cloud cover in southern China, which probably causes the overestimated 2-m temperature in southern China. Our study empha-sizes that, in such high-resolution-model studies for East Asia, special attention should be paid to the near-surface winds over the Hengduan Mountains.

1 Introduction

The Hengduan Mountains, on the southeastern edge of the Tibetan Plateau (TP), is a large, north–south-oriented range of mountains with complex topography that acts as an effec-tive separation between the lowlands of northern Myanmar and the lowlands of the Sichuan Basin. They serve as an effectual blocking of the movement of westerly wind in the lower troposphere towards East China (17.5°–45.5° N, 100°–125° E). This westerly wind transports atmospheric water from the Bay of Bengal to East China (Zhou and Yu 2005). The topography is fairly complex over the Hengduan

* Jingwei Xu
xu_jw@sina.cn

1 Key Laboratory of Meteorological Disaster, Ministry of Education (KLME)/Joint International Research Laboratory of Climate and Environment Change (ILCEC)/Collaborative Innovation Center on Forecast and Evaluation of Meteorological Disasters (CIC FEMD)/Joint Center for Data Assimilation Research and Applications, Nanjing University of Information Sciences and Technology (NUIST), Nanjing 210044, China

2 Climate Service Center Germany (GERICS)/Helmholtz Zentrum Geesthacht (HZG), 20095 Hamburg, Germany

3 Max Planck Institute for Meteorology, Bundesstrasse 53, 20146 Hamburg, Germany

4 MARUM Center for Marine Environmental Sciences, Bremen, Germany

5 Alfred Wegener Institute (AWI), 27568 Bremerhaven, Germany

6 Russian Academy of Science, Shirshov Institute of Oceanology, 36 Nahimovskiy Prospect, Moscow 117997, Russia

7 Meteorological Bureau of Jiangsu Province, Nanjing 210008, China

8 Center for Earth System Research and Sustainability, CliSAP, University of Hamburg, 20144 Hamburg, Germany

Mountains. Rivers in this region are narrow and steep. They feature typical "V"-shaped and deep canyons, among which the Tiger Leaping Gorge is a famous example. Owing to the friction generated by the complex topography and north–south-oriented range, these mountains are a source region for low-level vortices, such as the Southwest Vortex (Wang and Tan 2014). Therefore, the Hengduan Mountains are an important aspect of studying the circulation of water and heavy rain in East Asia.

Regional climate models (RCMs) are important research tools for studying the climate over areas with complex topography. Typically, the horizontal resolution of atmospheric general circulation models is about 150 km; however, the information required locally to achieve effective mitigation and adaptation measures needs be available at much finer scales, down to a resolution of 1 km or more (Koldunov et al. 2016). Regional downscaling using an RCM can provide a better spatial representation of atmospheric variables locally, but experiments over sufficiently long time periods and high enough horizontal resolutions (10 km or more) remain scarce, having only recently become operationally possible with the development of faster algorithms and more powerful supercomputers. Only under high horizontal resolution simulations can RCMs resolve narrow and steep valleys and thus help us to uncover the physical mechanisms at play in these regions of complex topography.

The REMO RCM (Jacob et al. 2007; Jacob et al. 2012; Jacob and Podzun 1997; Sein et al. 2015) has been shown to be relatively accurate in simulating the transport of atmospheric water vapor. One of the reasons is that REMO uses improved physical parameterizations from versions 4 and 5 of the ECHAM global climate model (Roeckner et al. 1996; Roeckner et al. 2003). Based on previous studies, we can state with relative certainty that REMO is able to capture well the cycles of precipitation and temperature over East Asia. For example, Zhang et al. (2005) found that REMO can capture the features of atmospheric circulation over East Asia in the years 1980 and 1990 and successfully reproduce the spatial distribution and seasonal variances of precipitation in East Asia. Jacob et al. (2012) used REMO with a horizontal resolution of $0.44° \times 0.44°$ to preform simulations over the South Asia domain, partly covering China, and concluded that the model is able to capture the mean annual cycles of precipitation and temperature in this region. Furthermore, at a horizontal resolution of 50 km, REMO can reproduce the main characteristics of South Asian summer monsoon circulation in the lower, middle, and upper troposphere (Saeed et al. 2012). And lastly, Kumar et al. (2014) found that a warm bias in the monsoon climate region of North India can be reduced by 1–3 °C by modifying the soil thermal characteristics.

Recently, Xu et al. (2018) identified the main mechanisms responsible for the colder and dryer climates over the TP in high-resolution REMO simulations relative to lower-resolution simulations. They found that 2-m temperature differences are connected to the amount of water vapor transported to the TP. In this study, we trace this water vapor transport around the TP and evaluate the downstream effects of the Hengduan Mountains in East China.

As a contribution to the activities of CORDEX (www.cordex.org), we validate REMO in terms of 2-m temperature over the East China region and analyze the main mechanisms behind the simulation differences at different horizontal resolutions. Specifically, we compare simulations using the current standard CORDEX resolution (about 25 km) and a lower horizontal resolution of about 50 km.

To investigate the performance of a higher model resolution and its effects on 2-m temperature, we concentrate on the following topics:

- Validating the 2-m temperature over East China simulated by REMO and revealing the differences between seasons;
- Evaluating the differences in REMO's performance between the high- and low-resolution simulations during different seasons over East China;
- Demonstrating the possible mechanisms leading to the unexpectedly poor performance in the high-resolution simulation.

The remainder of the paper is structured as follows: Sect. 2 describes the validation data, model, experimental setup, and interpolation method. In Sect. 3, we report on the validation of the 2-m temperature and wind field simulated by REMO over East China, with particular emphasis on elucidating the mechanisms behind the 2-m temperature simulation performance differences. The main conclusions and a discussion are presented in Sect. 4.

2 Model, data, and experimental setup

2.1 Model and simulation design

REMO (Jacob et al. 2012; Jacob et al. 2013; Sein et al. 2015) has been shown to be useful in simulating regional circulation and has been widely used in regional climate studies. Here, we use it to produce historical simulations under different horizontal resolutions over East Asia. The model is run using lateral boundary conditions from the European Centre for Medium-Range Weather Forecasts interim reanalysis (ERA-Interim; Dee et al. 2011), whose data have been documented to offer advanced performance over the TP with respect to temperature (Wang and Zeng 2012), the climatological water cycle, and climate trends (Gao et al. 2014; Xu et al. 2018), compared with other reanalysis data.

Our setup of REMO follows that of previous work (e.g., Déqué et al. 2007; Jacob 2001; Jacob et al. 2012; Jacob et al.

Fig. 1 Model domain and topography

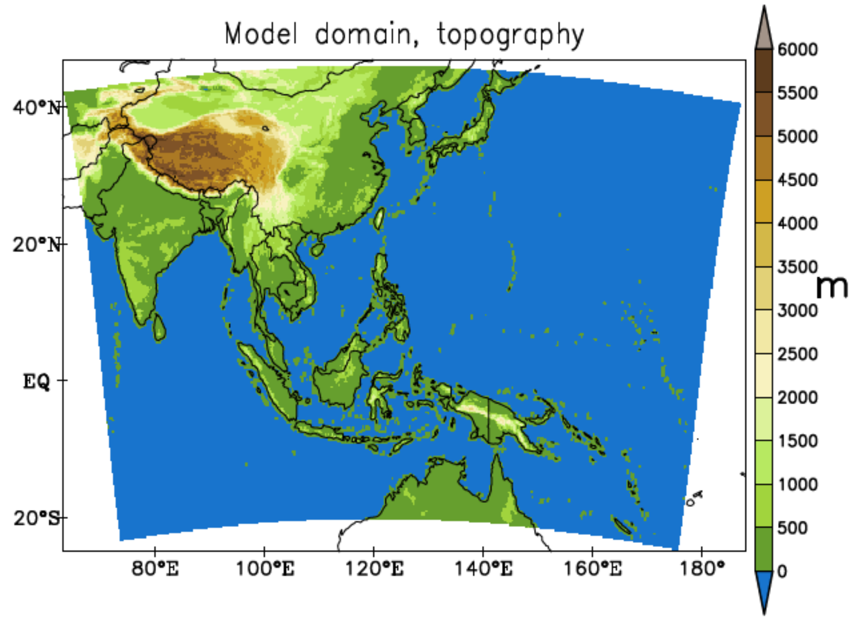

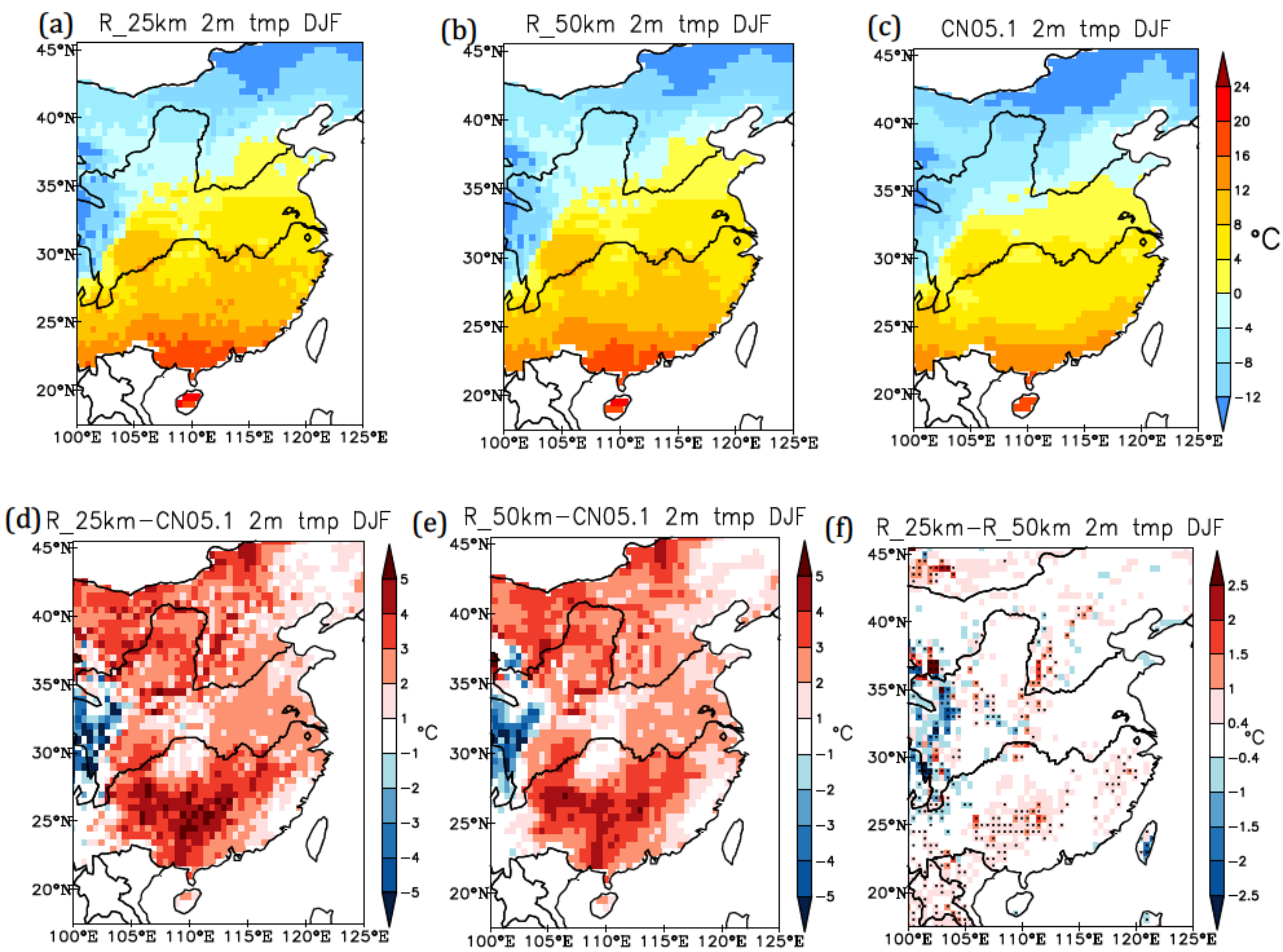

Fig. 2 Spatial distribution of the monthly mean 2 m temperature in DJF in **a** R_25km, **b** R_50km, and **c** CN05.1, seasonally (DJF). Averaged 2 m temperature bias for **d** R_25km, **e** R_50km, and **f** differences of the 2 m temperature between R_25km and R_50km during 1980 2012. The dotted regions denote 2 m temperature that is statistically significant at the 95% confidence level, based on the Mann Whitney *U* test. The main rivers (Yangtze and Yellow) are drawn as black lines, crossing west to east

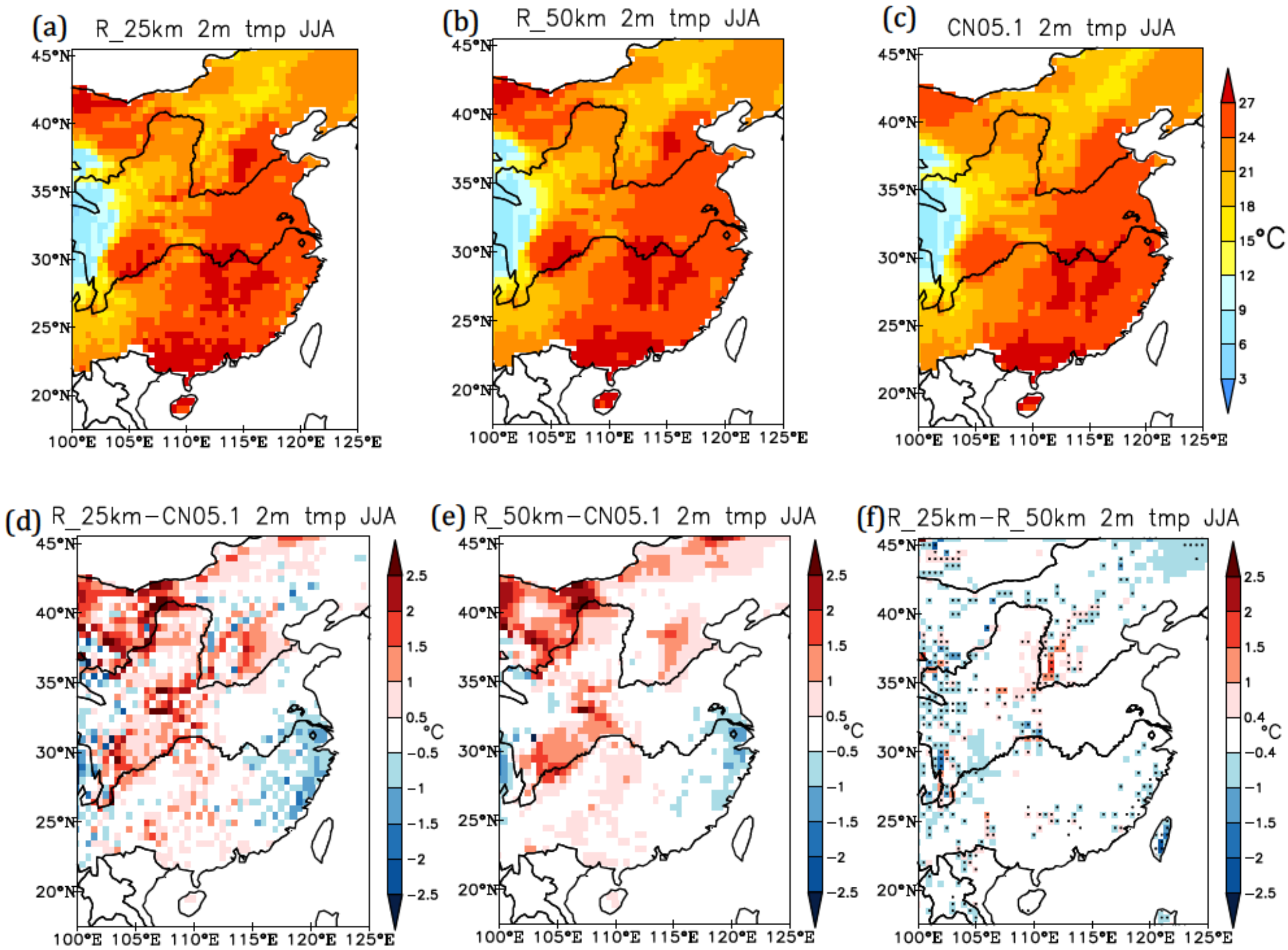

Fig. 3 As in Fig. 2 but for JJA

2001; Jacob et al. 2013). The dynamical core of REMO is based on the Europa-Modell of the German Weather Service (Majewski 1991), while its physical parameterizations are from versions 4 and 5 of the ECHAM global climate model (Roeckner et al. 1996; Roeckner et al. 2003). An Arakawa C-grid is used, and the horizontal grid boxes are on a rotated spherical grid (Simmons and Burridge 1981). The cumulus parameterization is based on the Tiedtke comprehensive mass flux convection scheme (Tiedtke 1989), and the Ritter and Geleyn (1992) radiation scheme is also applied. Also, REMO uses a "leap frog" scheme with semi-implicit correction and time filtering (Asselin 1972). To avoid boundary issues in the model and referring to the Davies relaxation scheme, no nudging is performed outside the eight points at the model lateral

Table 1 The 2 m temperature field seasonal mean bias from simulations

	Mean			Bias			RMSE			CORR		
	DJF	JJA	Ann	DJF	JJA	Ann	DJF	JJA	Ann	DJF	JJA	Ann
CN05.1	0.43	22.08	11.31									
R_25km	1.68	22.42	12.45	2.11	0.34	1.14	2.16	0.46	1.17	0.97	0.99	0.98
R_50km	1.55	22.48	12.34	1.98	0.40	1.03	2.02	0.50	1.07	0.97	0.99	0.98

CN05.1 is the average temperature over the whole of East China; the bias and RMSE values summarize the errors in the CN05.1 reanalysis dataset as the references at all grid points over East China; CORR is the correlation coefficient for the precipitation between CN05.1 and simulations. All CORR values are above the 95% confidence level

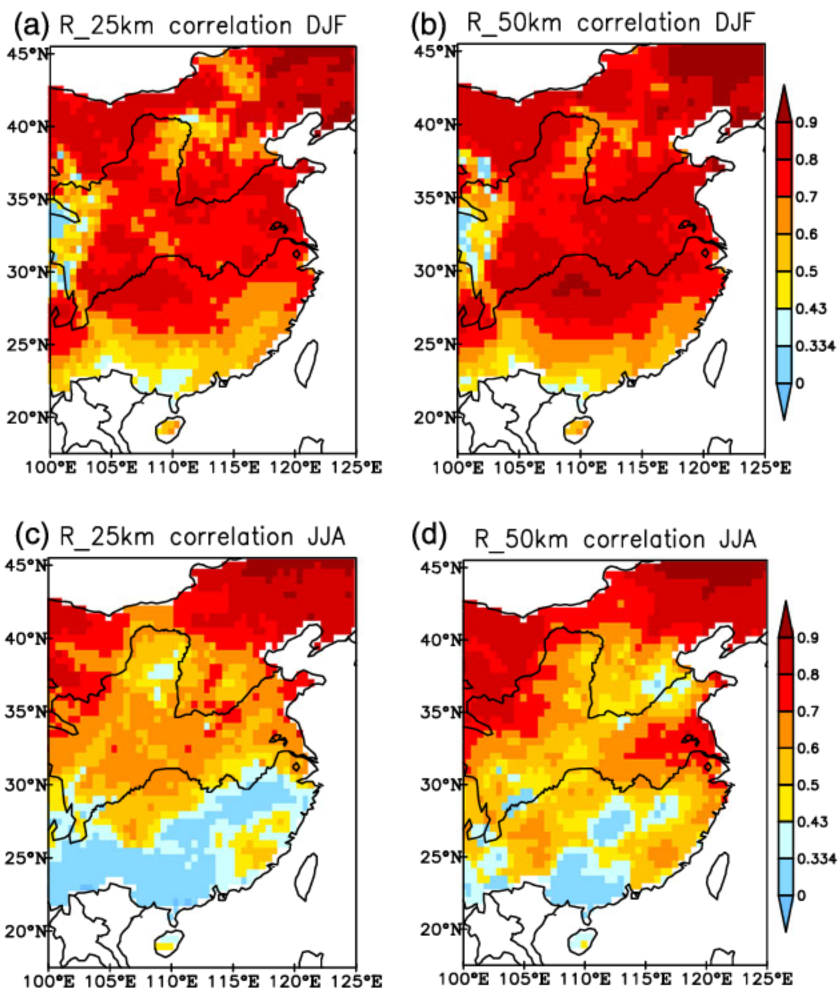

Fig. 4 Spatial distribution of monthly mean 2 m temperature temporal correlation coefficients in DJF in **a** R_25km and **b** R_50km during the period 1980 2012. **c**, **d** As in **a**, **b** but for JJA. The value of 0.334 is the threshold for statistical significance at the 95% confidence level; 0.43 is the threshold for statistical significance at the 99% confidence level

boundaries (Davies 1983). The atmosphere in REMO is separated into 27 hybrid vertical layers, where the top layer is at 10 hPa. The integration time step is 120 s for the 25-km horizontal resolution and 240 s for the 50-km one. The simulation period for the present study is 1980–2012, and the simulation domain includes the CORDEX East Asia domain (Fig. 1).

In order to make sure that the grid boxes in the 25- and 50-km resolution setups represent the same surface boundary

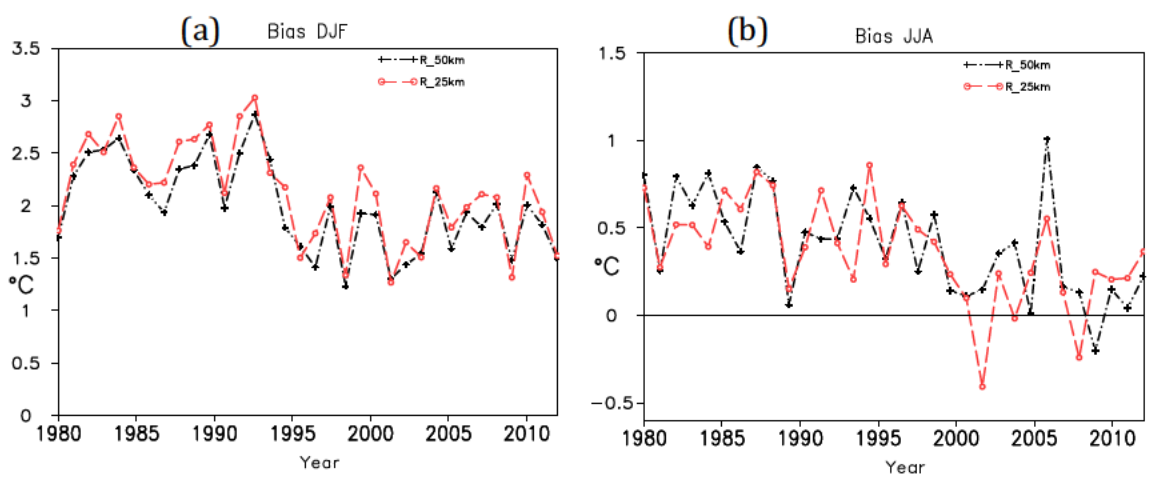

Fig. 5 Variances of 2 m temperature field mean bias for both simulations in **a** DJF and **b** JJA during 1980 2012

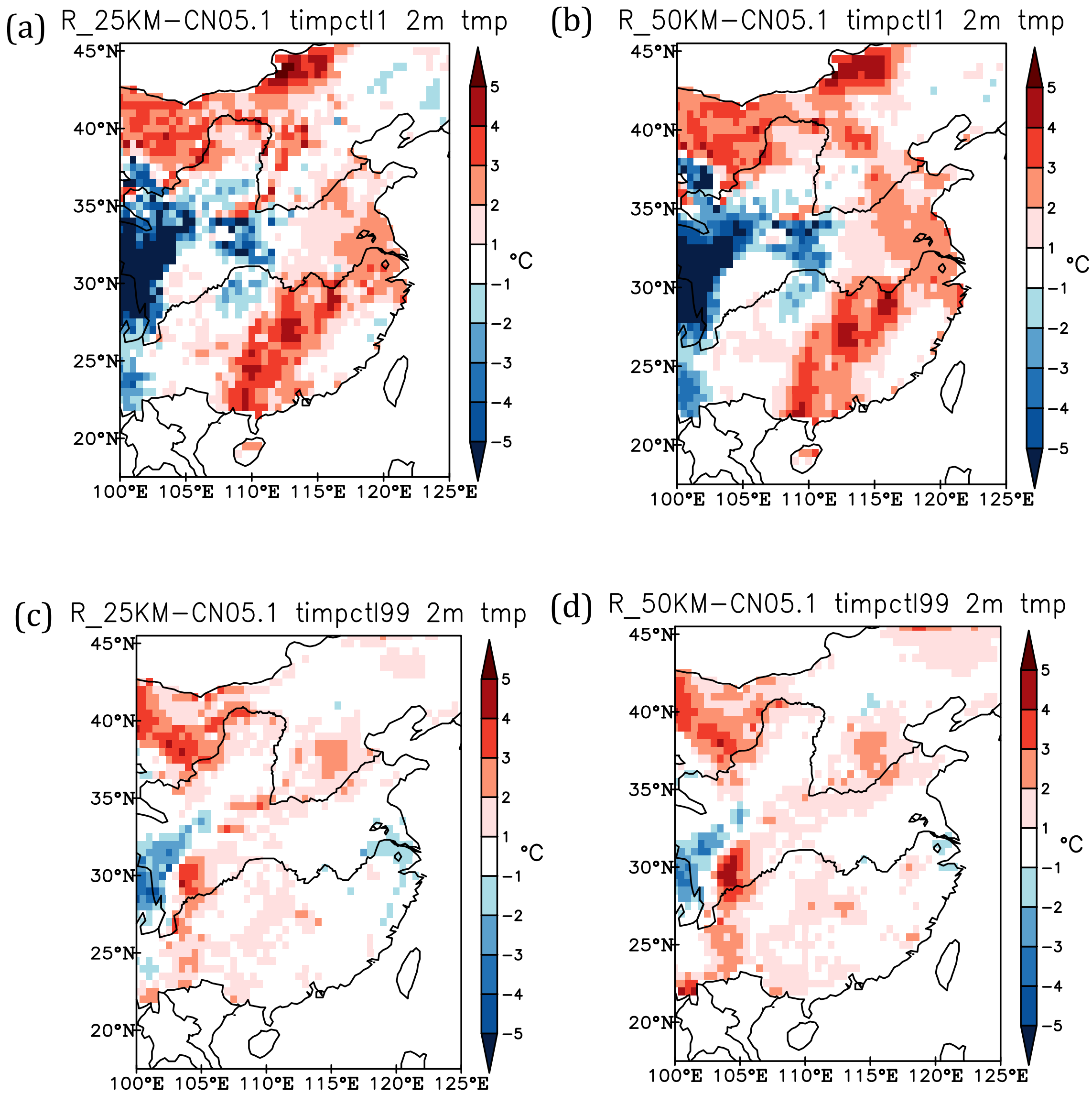

Fig. 6 Spatial distribution of the extremely low 2 m temperature bias (1st percentile) in **a** R_25km and **b** R_50km. **c**, **d** As in **a**, **b**, but for the 99th percentile based on daily mean 2 m temperature during 1980 2012

conditions—for example, the land–sea mask and soil texture—the grid is constructed in such a way that four grid boxes from the 25-km configuration exactly overlay one from the 50-km configuration, meaning there is no position shift between the four 25-km boxes and the one 50-km box. The same sources are used for preparing the land surface parameters. The land surface albedo is based on 50-km resolution data (Rechid et al. 2009), as are the soil texture data; therefore, for these two datasets, there is no difference between the 50- and 25-km configurations. The land surface data are based on Hagemann et al. (1999) and Hagemann (2002), and the resolution is 1 km. The orographic data are from the Global 30 Arc-Second Elevation Data Set (GTOPO30). The land surface characteristics are then aggregated to the target resolution. Compared with the magnitude of the orography differences, there are only a few differences between the 25- and 50-km configurations in terms of the land surface/vegetation. In summary, while there are differences between the 25- and 50-km configurations in terms of the land surface/vegetation characteristics, the major differences in this region are due to differences in orography.

Considering more sub-grid-scale properties can be represented on a high-resolution grid, the added value of a high-resolution simulation is more obvious on such a grid (Prein 2016). However, comparison on a coarse grid can be reasonable, because both resolutions are able to distinguish the analyzed features (Casanueva et al. 2015). Thus, no artificial values need to be added when interpolating high-resolution data to coarser resolutions. After careful consideration, the analyses and comparisons in this study are carried out at the coarser resolution (50 km × 50 km). In this paper, we refer to the 25 km × 25 km resolution simulation as R 25km and the

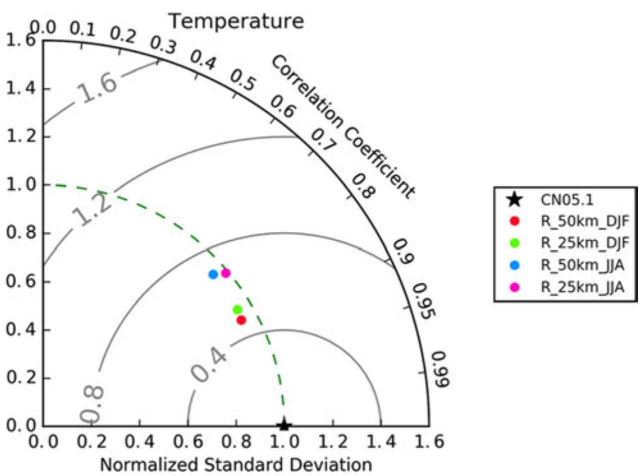

Fig. 7 Taylor diagram of the 2 m temperature over East China during 1980 2012. All points are statistically significant in their correlation at the 95% confidence level, based on the two tailed *t* test, with CN05.1 observations as the reference

50 km × 50 km resolution simulation as R 50km. The two experiments, R 25km and R 50km, are run simultaneously without further nesting.

2.2 Observations

The reference gridded 2-m temperature observations are from the Beijing Climate Center of the China Meteorological Administration. The dataset is called China Daily Gridded Surface Air Temperature, version 5.1 (CN05.1; Wu and Gao 2013; Xu et al. 2009) and has a spatial resolution of 0.25° × 0.25°. To produce the data, the climatology was first interpolated by thin plate smoothing splines, and then a gridded daily anomaly derived from the angular distance weighting method was added to the climatology to obtain the final product (Xu et al. 2009). CN05.1 was generated based on temperature observations from 2400 observation stations in China from 1961 to 2012.

2.3 Methods

The first-order conservative interpolation method (Redler 2015) is used to interpolate the simulation results and observations to the R 50km grid. Because of the different representations of orography in the R 25km, R 50km, and CN05.1, a lapse rate of 0.0064 °C/m is used to transfer the 2-m temperature to the same height for intercomparison. The region of analysis covers East China, which is the area over (17.5°–45.5°N, 100°–125°E), and only characteristics during boreal winter, defined as December–January–February (DJF), and summer, defined as June–July–August (JJA), are analyzed. To present the differences between the simulations and observations, the Taylor diagram (Taylor 2001) is used; and to detect the statistical significance of the differences, at the 95% confidence level, the Mann–Whitney *U* test is used. The mean, bias, root-mean-square-error (RMSE), and Pearson's spatial correlation coefficient are used as quantitative measures.

3 Results

3.1 Seasonal mean 2-m temperature bias over East China

The 2-m temperature distributions over East China show two distinct seasons: winter and summer (Figs. 2 and 3, respectively). The coldest area in DJF is the Inner Mongolian Plateau in Northeast China (Fig. 2c), and the warmest areas in JJA are the middle reaches of the Yangtze River and Hainan in southern China (Fig. 3c). Both simulations generally capture the spatial pattern of 2-m temperature

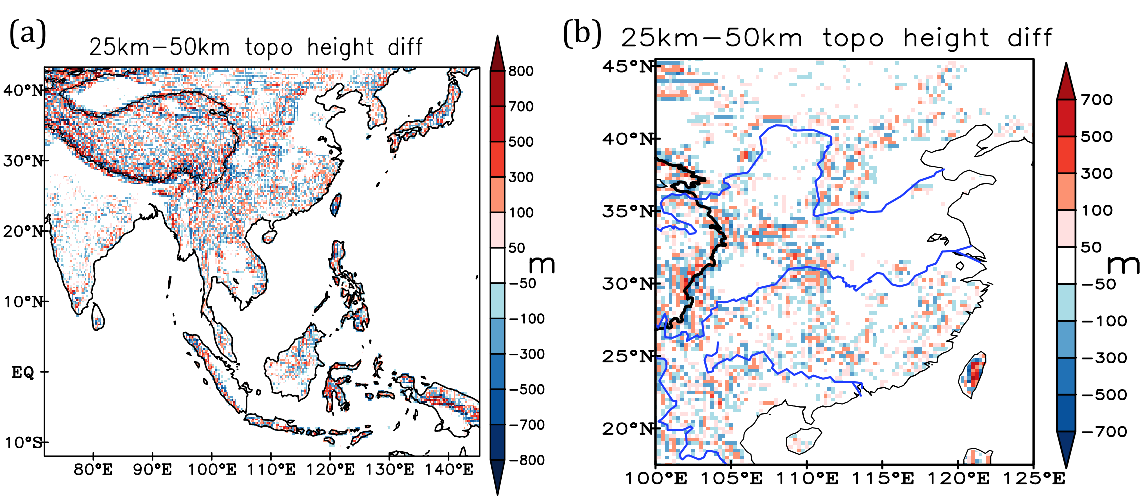

Fig. 8 Differences in orography from the R_25km and R_50km simulations over **a** the whole domain and **b** East China. The solid black line is the 3000 m a.s.l. contour line over the TP. The main river valleys are shown as blue lines

well. They also capture the seasonal cycle remarkably well (Figs. 2d, e and 3d, e), but significant warm biases are evident during winter over southern China. Both simulations show similar spatial correlation to observations (Table 1).

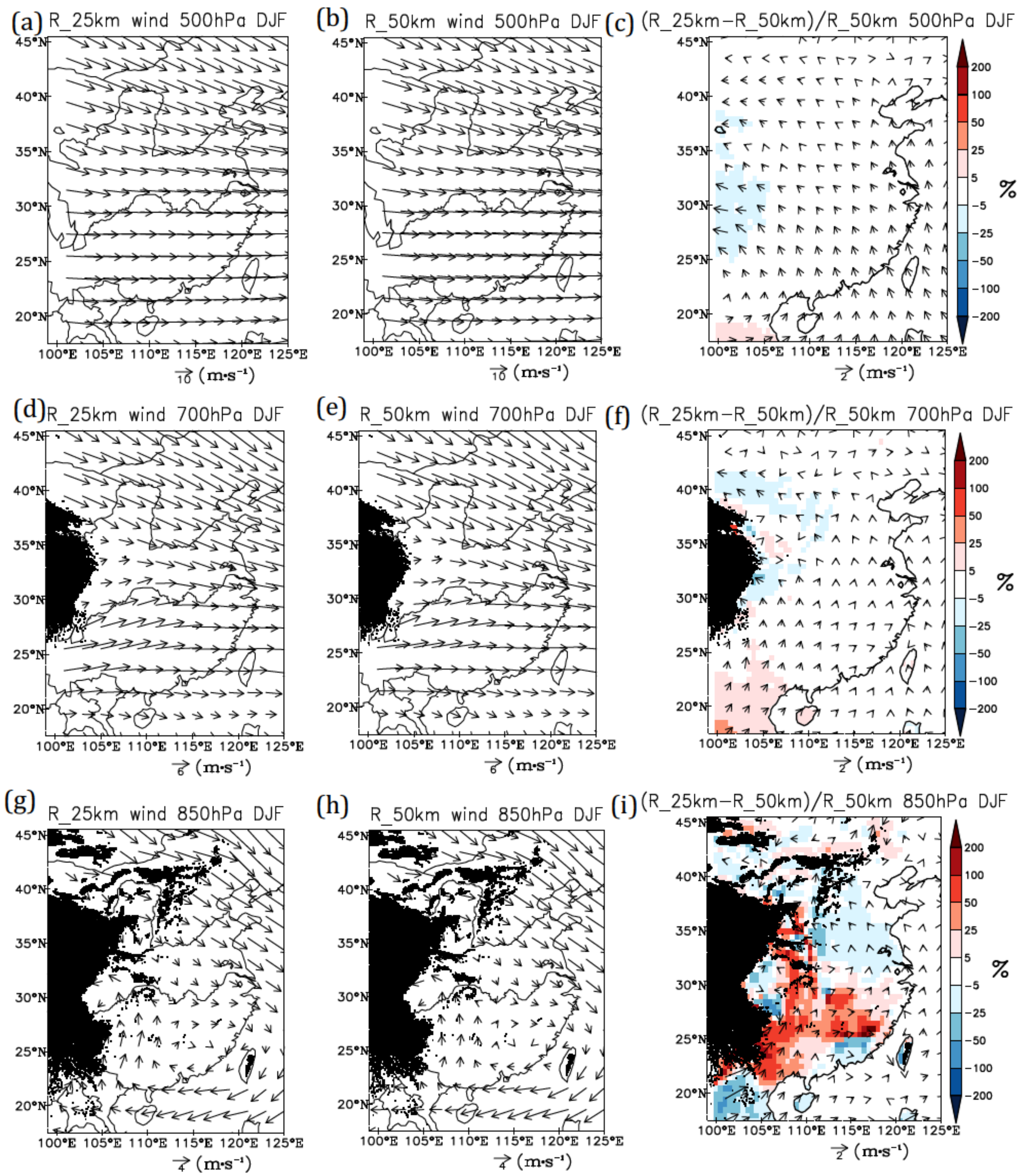

Fig. 9 Flow patterns of the wind at **a** 500, **d** 700, and **g** 850 hPa in R_25km. **b, e, h** As in **a, d, g** but for R_50km. **c, f, i** As in **a, d, g** but for the relative differences in wind speed from R_25km and R_50km over East China in DJF. The direction (as streamlines) and speed difference (as colors) of the winds are shown. The shaded area indicates topography higher than 1500 or 3000 m at 850 and 700 hPa, respectively

In winter, although R 25km and R 50km show the same magnitude of warm biases all year round, the overestimation of 2-m temperature during DJF in R 25km is stronger than in R 50km (Fig. 2d, e). Over a large part of East China in DJF, the temporal correlation coefficient in R 50km is higher than that in R 25km, especially in southern China (Fig. 4a, b). The mean 2-m temperature field bias (Fig. 5a) shows that the R 25km and R 50km simulation biases are quite similar, but the R 50km bias is smaller compared to that in the high-resolution simulation (R 25km) for DJF. Due to better availability of observations, the 2-m temperature biases become smaller for the

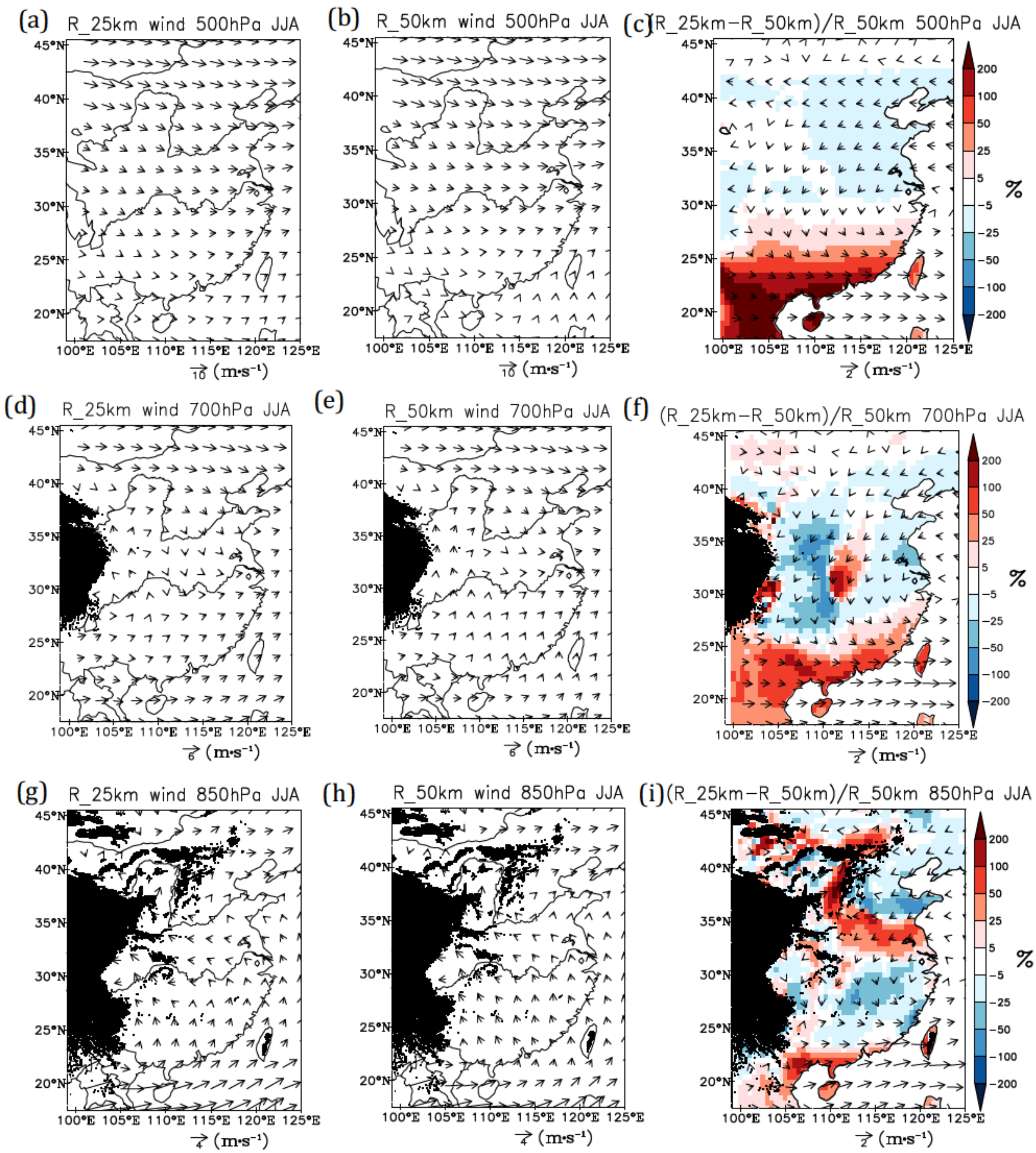

Fig. 10 As in Fig. 9 but for JJA

simulated recent years (Xu et al. 2009). A similar phenomenon is also apparent from the mean bias field and RMSE (Table 1). In general, both R 25km and R 50km capture the seasonal features, but the performance of R 25km is poor in DJF, especially in southern China.

In summer, the prevailing wind is southerly in southern China at 850 hPa, which means it comes directly from the sea. However, this wind is driven over the ocean by prescribed sea surface temperature from ERA-Interim, which is the same for R 25km and R 50km. As a result, the magnitude of the

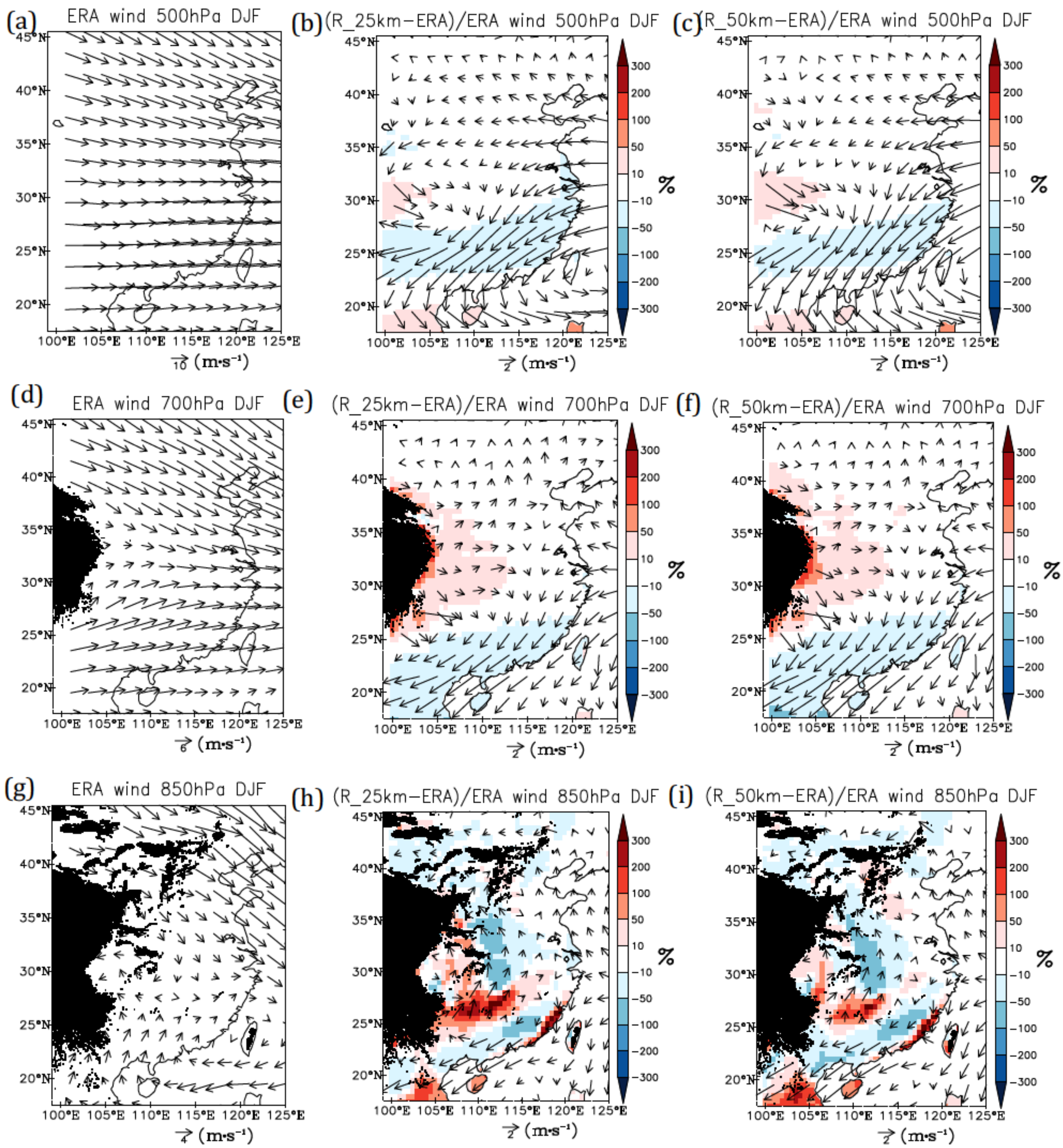

Fig. 11 Wind at **a** 500, **d** 700, and **g** 850 hPa in ERA Interim, used for validation of the model results. **b**, **e**, **h** As in **a**, **d**, **g** but for the relative differences in wind speed from ERA Interim and R_25km. **c**, **f**, **i** As in **a**, **d**, **g** but for the relative differences in wind speed from ERA Interim and R_50km over East China in DJF. The direction (as streamlines) and speed difference (as colors) of the winds are shown. The shaded area indicates topography higher than 1500 or 3000 m at 850 and 700 hPa, respectively

differences is lower in JJA than in DJF. Although R 25km and R 50km show the same magnitude of biases, the latter overestimates the 2-m temperature in Central and North China to a greater extent than R 25km (Fig. 3d, e). The temporal correlation coefficient in R 50km is higher than in R 25km only in southern China (Fig. 4c, d), whereas R 25km produces higher correlation coefficients with observations over large areas, like the middle reaches area between the Yangtze River and Yellow River. The 2-m temperature field mean bias (Fig. 5b) shows that R 25km is closer to observations in summer. The temperature field mean bias and RMSE in JJA show an advantage of the R 25km simulation over the R 50km one (Table 1).

Since the R 25km simulation overestimates the southwesterly wind more than the R 50km simulation in DJF at 850 hPa, which will be discussed in detail in the next section, R 25km

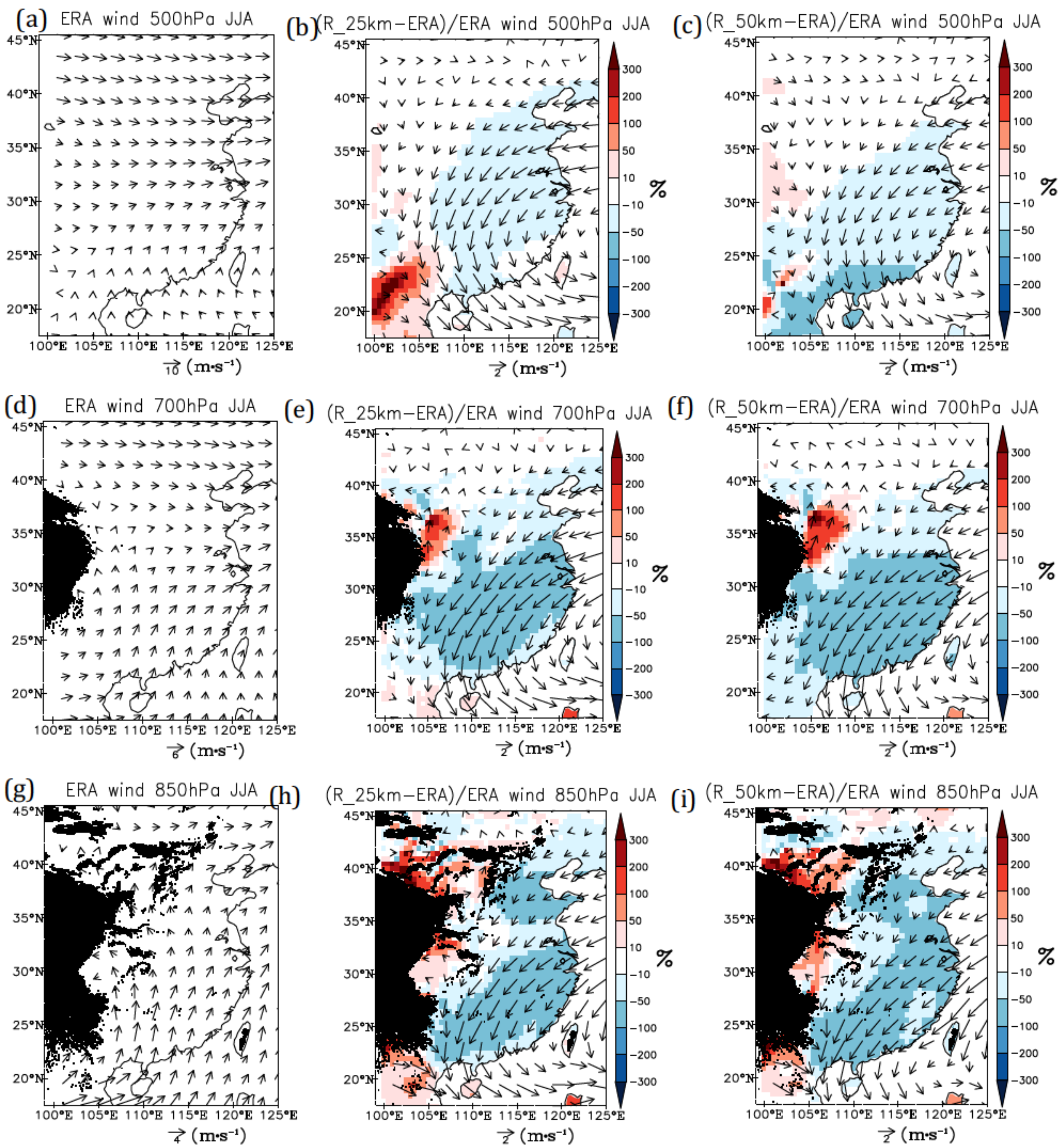

Fig. 12 As in Fig. 11 but for JJA

shows a higher warm bias during extreme cold events (1st percentile, based on daily mean temperature; Fig. 6a, b). Many studies have shown that high-resolution simulations are better at reproducing extreme events, especially in summer (Borscheid 2015; Jacob et al. 2014; Luca et al. 2012; Lucas-Picher et al. 2012). Here, R 25km shows smaller biases than R 50km during extremely hot events (99th percentile) in large areas of South, Central and Northeast China (Fig. 6c, d).

To summarize the results in this section, we plot a Taylor diagram (Taylor 2001). The Taylor diagram (Fig. 7) shows that: (1) in DJF, the coarse resolution is unexpectedly closer to observations, especially in southern China; and (2) in JJA, considering results over the whole of East China, the high-resolution simulation shows sizeable advantages over the coarse resolution.

Recent studies demonstrate that high-resolution simulations show added value to coarse resolution simulations (Casanueva et al. 2015; Luca et al. 2012; Lucas-Picher et al. 2012). Contrary to our expectations that the high resolution should show distinctive advantages over the coarse resolution, the high-resolution setup of REMO does not perform as well as the coarse resolution during DJF over East China, especially over southern China.

3.2 Probable cause of the overestimated near-surface air flow over the Hengduan Mountains

Many studies have shown that model performance can be improved by increasing the resolution for better resolved topography, resulting in more realistic near-surface air flow simulation, especially in regions with complex topography (Gao et al. 2006; Gao et al. 2015a; Gao et al. 2015b; Xu et al. 2018). More realistic topography can influence the air flow near the land surface through a dynamical process, and change the amount of atmospheric water vapor carried by the air flow, leading to an adjustment in total cloud cover, which triggers the net radiation differences.

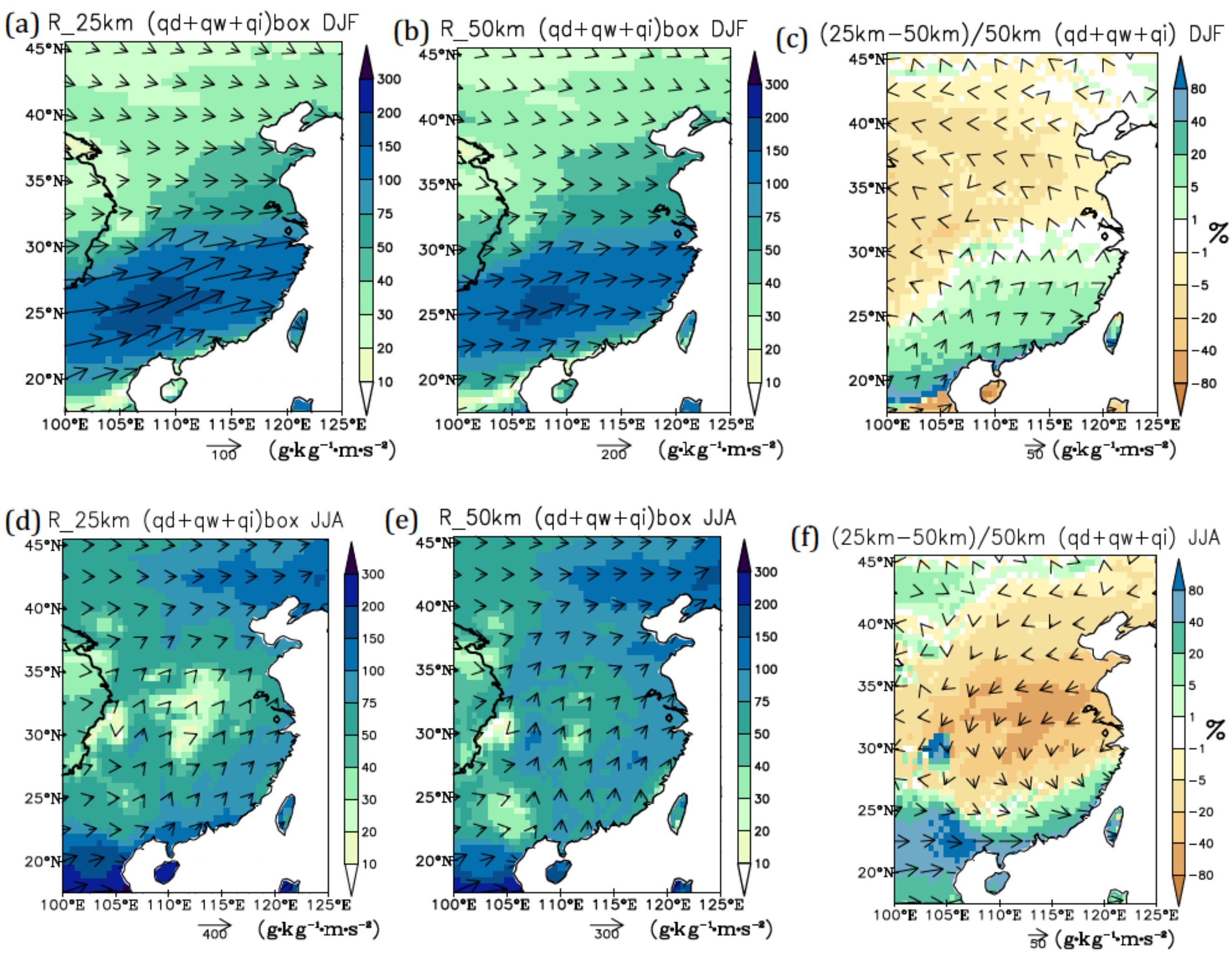

Fig. 13 Basic flow of the integrated components of water transport over the whole air column from **a**, **d** R_25km, **b**, **e** R_50km, and **c**, **f** their differences. The flow direction is shown by the arrows and the flow value by colors

In order to eliminate other factors, special care is paid to the preparation of the surface forcing over land (e.g., vegetation characteristics, soil texture) in such a way that they are the same in our two experiments, i.e., R 25km and R 50km. There are differences between the 25- and 50-km configurations in terms of land surface/vegetation characteristics, but the major differences in this region are due to orography.

Interpolation errors can sometimes be more significant than the differences in topography. This is why we apply the nearest neighbor remapping method in this next part of our study, in which the topography is directly remapped from the 50- to the 25-km grid, retaining as much of the original pattern as possible. The topographical differences are huge in areas of complex topography, e.g., at the edges of the TP, especially over the Hengduan Mountains (Fig. 8a). The valleys are enlarged in the R 25km simulation compared to the R 50km one (Fig. 8b), leading to a weakened blocking effect of the Hengduan Mountains (Xu et al. 2009).

In the Hengduan Mountains, the prevailing winds in DJF at 850 hPa are southwesterly, whereas in JJA the westerly winds weaken substantially (Wang and Tan 2014). Since the Hengduan Mountains are mainly oriented in the north–south direction, they block the westerly winds. Due to the weakened blocking effect in R 25km, the near-surface southwesterly wind increases over the Hengduan Mountains (Fig. 9f, i). The magnitude of the airflow differences reduces with height, being negligible at 500 hPa in DJF (only 5%; Fig. 9c), but still relatively high in JJA since more convection happens during JJA in R 25km in southern China (Fig. 10c, f, i).

Since the wind differences play a key role in the proposed mechanism, we validate the wind in the middle and lower troposphere. As shown previously, REMO can capture the basic flow over East China (Jacob et al. 2012; Xu et al. 2018; Zhang et al. 2005), and we also find that the basic flows in R 25km and R 50km share a similar pattern as that in ERA-Interim. The wind bias decreases with increasing height, with the greatest wind bias happening at 850 hPa. It is worth

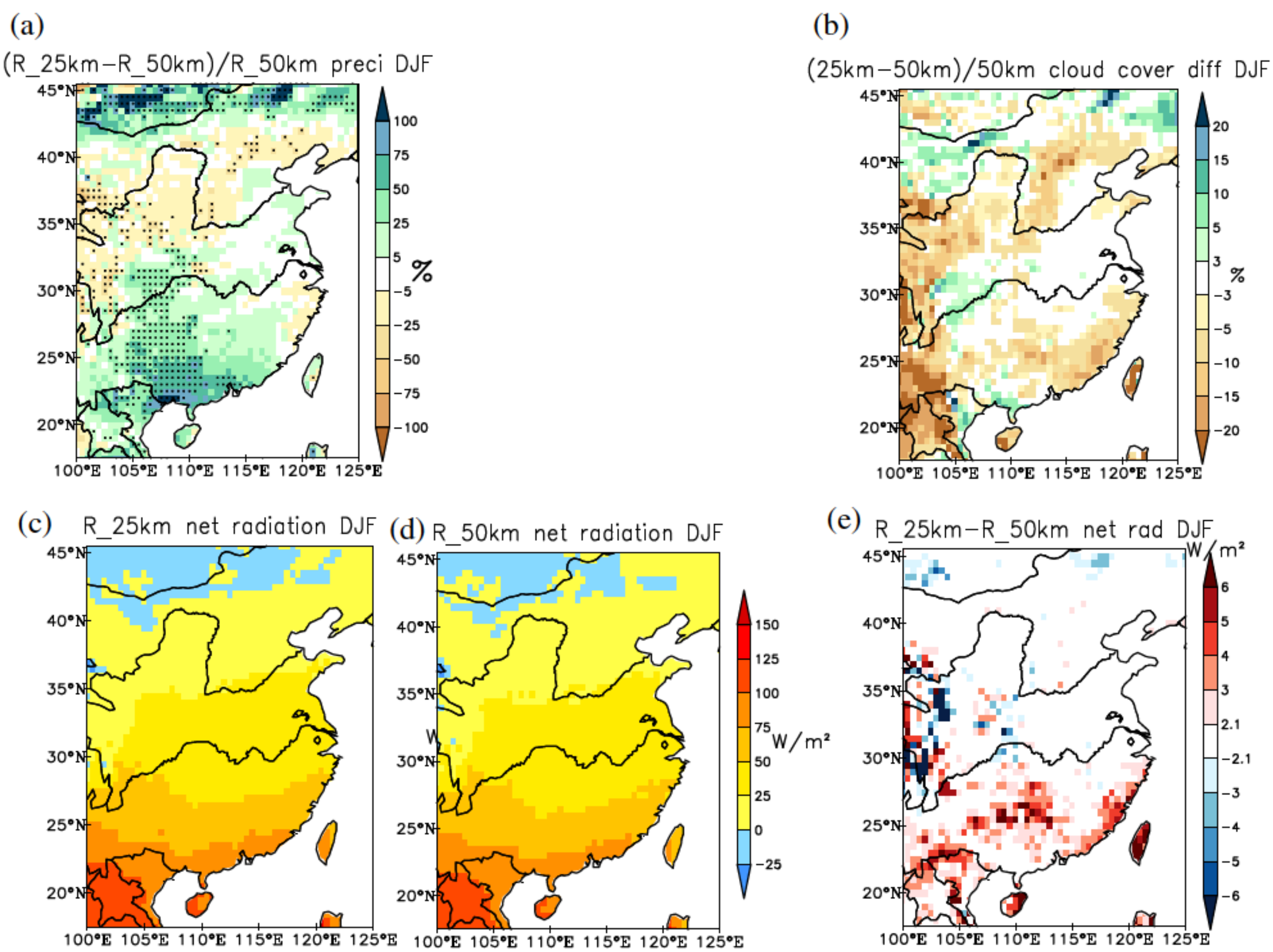

Fig. 14 Differences in **a** monthly mean precipitation and **b** total cloud cover between R_25km and R_50km in DJF during 1980 2012. The dotted regions denote precipitation that is statistically significant at the 95% confidence level, based on the Mann Whitney *U* test. **c** **e** Spatial distribution of monthly mean net radiation in **c** R_25km, **d** R_50km, and **e** their differences in DJF during 1980 2012

mentioning that the near-surface westerly wind biases are overestimated in R 25km compared to R 50km in DJF at 850 hPa (Fig. 11a–f). However, since the prevailing westerly wind in JJA is substantially weakened, there is only a limited influence from the Hengduan Mountains, which possibly gives rise to a sizeable advantage in JJA over southern China in R 25km (Table 1). In JJA, the wind biases in R 25km mainly show improvements at all analyzed levels (Fig. 12).

3.3 Possible mechanism behind the overestimated westerly wind influence in downstream areas

As compared with ERA-Interim wind, the southwesterly wind is overestimated and affects the 2-m temperature results in DJF in southern China. When the westerly wind is substantially weakened in JJA, R 25km shows a sizeable advantage at 850 hPa in JJA (Table 1). The key overestimated southwesterly wind influences the downstream area, such as southern China, though a dynamic process that can be described as follows.

For the most part, atmospheric water is transported in the middle and lower troposphere. Hence, the Hengduan Mountains, with an average height of around 4000 m a.s.l. (above sea level), can effectively influence the atmospheric water transport to downstream areas, such as southern China. We use the simulated values of water transport in the whole air column, comprising vapor, liquid water, and ice, to analyze these effects. The results show that the atmospheric water has a robust link with the airflow at 850 and 700 hPa (Fig. 13c, f). As a result of stronger southwesterly wind, there is an increase in atmospheric water transported by the airflow in DJF, leading to elevated precipitation in southern China, but a reduction over northern China and over the TP (Figs. 14 and 15a). This leads to reduced cloud cover, and subsequently a larger net radiation increase over almost the entire region of southern China and part of Northeast China in DJF.

The relationship between cloud and precipitation differs between 30°–40° N and 20°–30° N. Since convective activity is defined by the convective available potential energy, when the atmospheric moisture is high, convection is more easily initiated (Roeckner et al. 2003). In the region between 20° N and 30° N, the moisture comes from the Indian Ocean (Zhou and Yu 2005) and is abundant compared with the region between 30° N and 40° N (Fig. 13a, b). In the moisture-abundant region, the precipitation process takes place quickly. Cloud can exist for only a relatively short time, which means more precipitation and less cloud cover. Whereas, in the moisture-lacking region between

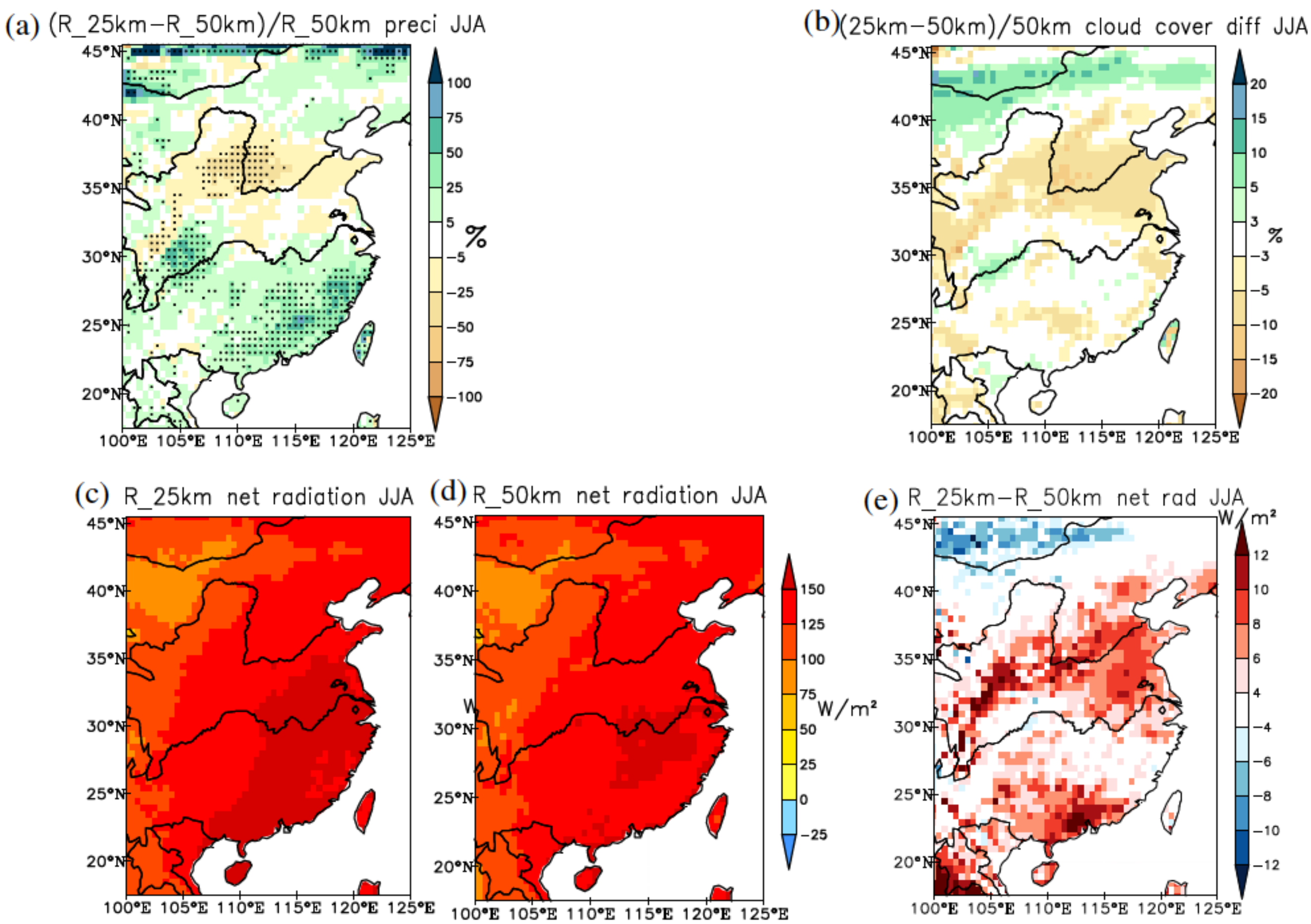

Fig. 15 As in Fig. 14 but for JJA

30° N and 40° N, the moisture mainly comes from West China, an arid region, where the precipitation is fairly limited and cloud cover can indicate advected atmospheric moisture. The process of precipitation takes place relatively slowly. So, a sizeable positive correlation between cloud cover and precipitation means less cloud cover and less precipitation. The cloud cover has a positive connection with the net radiation.

To further confirm the connection between the net radiation differences and 2-m temperature differences, the correlation coefficients are shown. In both simulations, the net radiation correlation coefficient is higher than the temperature advection correlation coefficient over most parts of East China in DJF and JJA. Considering the altitude in the study region, the temperature advection is jointly determined by the temperature gradient and wind speed at 850 hPa. The temporal correlation coefficients show that the net radiation differences have a strong connection with the 2-m temperature differences in DJF (exceeding the 95% confidence level over large parts of East China; Fig. 16a) and in JJA in almost the entire study area (exceeding the 99% confidence level; Fig. 16c); yet only a few areas illustrate that the warm advection differences have a significant connection with the 2-m temperature differences in JJA (Fig. 16d). Furthermore, the area, where the temporal correlation between temperature advection differences and 2-m temperature differences (linking the increasing west wind speed and high 2-m temperature) passes the significance threshold of the 95% confidence level, covers almost the whole of the temperature difference boxes in DJF (Fig. 16b). With regard to the climatic circulation patterns, it is probably the overestimated wet southwesterly wind in R 25km that causes the greater 2-m temperatures in DJF over southern China.

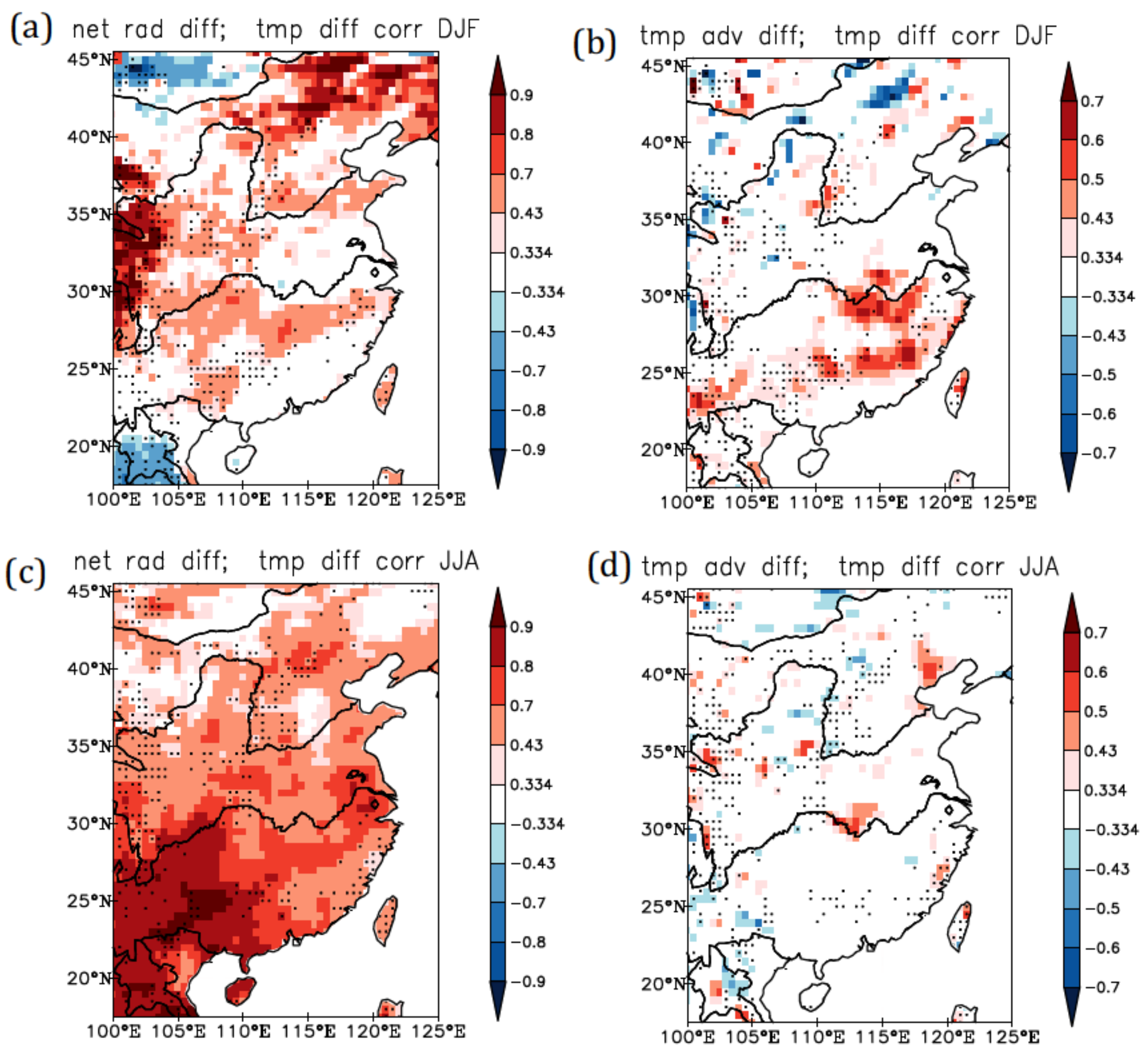

Fig. 16 Temporal correlation between the monthly mean 2 m temperature differences and net radiation in **a** DJF and **c** in JJA. **b**, **d** As in **a**, **c**, but for warm advection differences. The value of 0 334 (0.43) represents the threshold for significance at the 95% (99%) confidence level, based on the two tailed t test. The dotted regions denote 2 m temperature that is statistically significant at the 95% confidence level, based on the Mann Whitney U test. The net radiation is the sum of net shortwave radiation and net longwave radiation

4 Conclusions and discussion

The Hengduan Mountains are one of the most important atmospheric water transport passages to East China (Gao et al. 2015a; Gao et al. 2015b; Jacob et al. 2014; Xu et al. 2018) and one of the sources of low-level vortices, such as the Southwest Vortex (Wang and Tan 2014). However, there have been relatively few analyses of the downstream effects of this region with highly complex orography. Here, we identify the main mechanism behind overestimated air flow leading to differences in REMO simulations at resolutions of 25 and 50 km over East China. Results show that the high-resolution simulation tends to overestimate the near-surface wind over areas with complex topography. With the help of the overestimated southwesterly wind, the amplified atmospheric water vapor is transported to East China in the high-resolution simulation. Additionally, our study reveals the benefits gained by using a high resolution for 2-m temperature in JJA. Although we identify the main mechanism acting at the seasonal time scale, detailed analyses are still needed to study these effects on specific weather events. The major findings of our study can be summarized as follows:

(i) The 2-m temperature results from REMO simulations with horizontal resolutions of 25 and 50 km are validated against CN05.1 observations over East China. Results show that REMO can capture the spatial patterns of 2-m temperature reasonably well. For the mean 2-m temperature field comparison, the 2-m temperature at the coarse resolution is closer to the observations in DJF, whereas in JJA, the high resolution simulation shows a sizeable advantage over the coarse resolution. Similar results are obtained for extreme events (hot and cold), wherein the high resolution does not show its advantages in DJF, especially over southern China.

(ii) In our experiments, almost all the land parameters in REMO are the same; there are only a few differences between the 25- and 50-km configurations in terms of land surface/vegetation characteristics, but the major differences in this region are due to differences in orography. The greatest differences in topography occur in the complex topographical regions along the edges of the TP and the Hengduan Mountains. Due to the high sensitivity of R 25km to the weakened blocking effect over the Hengduan Mountains, R 25km tends to overestimate the near-surface southwesterly wind locally. Moreover, this overestimated wind influences the downstream area, e.g., southern China. Compared with the ERA-Interim wind field, the magnitude of the overestimated wind decreases with increasing height. With the help of the overestimated southwesterly wind, the amount of atmospheric water vapor carried by the wind is increased in R 25km. This leads to a statistically significant precipitation increase (statistically significant at the 95% confidence level, based on the Mann–Whitney *U* test) in southern China.

(iii) The main mechanisms behind the overestimated wind and 2-m temperature are as follows: In southern China, the moisture largely comes from the Indian Ocean and is abundant compared with the region between 30° N and 40° N. The process of precipitation takes place quickly in this area, where the cloud only exists over a relatively short time, which means more precipitation and less cloud cover. These features cause total cloud cover adjustment, leading to a variation in the net radiation distribution, largely over southern China. The net radiation differences have a robust connection with the 2-m temperature (statistically significant at the greater than 99% confidence level in JJA over most parts of East China).

To maintain a clear focus in this study, we mainly discuss the overestimated wind near the ground surface caused by the increased resolution of topography. Nonetheless, other physical processes, such as land–atmosphere interactions and convection-scheme choice, may influence the results. Although the downstream effect is a nonlinear process, it influences nearly all dynamic and thermodynamic processes. Moreover, the primary focus here is the connection between overestimated wind and 2-m temperature. This study emphasizes that, in such high-resolution studies in this region, special attention should be paid to the near-surface winds over the Hengduan Mountains. Furthermore, other mechanisms that are impacted by the relationship between atmospheric moisture and cloud cover are worthy of investigation in the future.

Acknowledgements We thank anonymous reviewers for comments and suggestions that helped to improve the manuscript. We thank the ECMWF and CMA for providing the gridded data. We thank the Climate System Department at GERICS for the consultations that took place regarding the REMO model. The simulations were carried out at the German Climate Computing Center (DKRZ).

Funding information This work is supported by a project entitled "Relationships between glacier changes and atmospheric circulation in High Mountain Asia," supported by the National Natural Science Foundation of China (Nos. 41871053, 41371095, 91337218), the China Special Fund for Meteorological Research in the Public Interest (No. GYHY 201406008), project S1 (Diagnosis and Metrics in Climate Models) of the Collaborative Research Centre TRR 181 Energy Transfer in Atmosphere and Ocean program funded by the German Research Foundation, EC project PRIMAVERA under grant agreement no. 641727, and the state assignment of FASO Russia (theme Nos. 0149 2019 0015, 0149 2018 0014). This study was also funded by "the Priority Academic Program Development of Jiangsu Higher Education Institutions" (PAPD).

Compliance with ethical standards

Conflict of interest The authors declare that they have no conflicts of interest.

References

Asselin R (1972) Frequency filter for time integrations. Mon Wea Rev
100:487 490

Borscheid P (2015) Temporal and spatial scaling impacts on extreme precipitation. Atmo Chem Phys 15:2157 2196

Casanueva A et al (2015) Daily precipitation statistics in a EURO CORDEX RCM ensemble: added value of raw and bias corrected high resolution simulations. Clim Dyn 31:1 19

Davies HC (1983) Limitations of some common lateral boundary schemes used in regional NWP models. Mon Weather Rev 111: 1002 1012

Dee DP, Uppala SM, Simmons AJ, Berrisford P, Poli P, Kobayashi S, Andrae U, Balmaseda MA, Balsamo G, Bauer P, Bechtold P, Beljaars ACM, van de Berg L, Bidlot J, Bormann N, Delsol C, Dragani R, Fuentes M, Geer AJ, Haimberger L, Healy SB, Hersbach H, Hólm EV, Isaksen L, Kållberg P, Köhler M, Matricardi M, McNally AP, Monge Sanz BM, Morcrette JJ, Park BK, Peubey C, de Rosnay P, Tavolato C, Thépaut JN, Vitart F (2011) The ERA interim reanalysis: configuration and performance of the data assimilation system. Q J R Meteorol Soc 137:553 597

Déqué M, Rowell DP, Lüthi D, Giorgi F, Christensen JH, Rockel B, Jacob D, Kjellström E, de Castro M, van den Hurk B (2007) An intercom parison of regional climate simulations for Europe: assessing uncer tainties in model projections. Clim Chang 81:53 70

Gao X, Xu Y, Zhao Z, Pal J, Giorgi F (2006) On the role of resolution and topography in the simulation of East Asia precipitation. Theor Appl Climatol 86:173 185

Gao Y, Cuo L, Zhang Y (2014) Changes in moisture flux over the Tibetan Plateau during 1979 2011 and possible mechanisms. J Clim 27: 1876 1893

Gao Y, Leung LR, Zhang Y, Cuo L (2015a) Changes in moisture flux over the Tibetan Plateau during 1979 2011: insights from a high resolution simulation. J Clim 28:4185 4197

Gao Y, Xu J, Chen D (2015b) Evaluation of WRF mesoscale climate simulations over the Tibetan Plateau during 1979 2011. J Clim 28:2823 2841

Hagemann S (2002) An improved land surface parameter dataset for global and regional climate models. Report 336, Max Planck Institute for Meteorology, Hamburg

Hagemann S, Botzet M, Dümenil L, Machenhauer B (1999) Derivation of global GCM boundary conditions from 1 km land use satellite data. Report 289, Max Planck Institute for Meteorology, Hamburg

Jacob D (2001) A note to the simulation of the annual and inter annual variability of the water budget over the Baltic Sea drainage basin. Meteorog Atmos Phys 77:61 73

Jacob D, Bärring L, Christensen OB, Christensen JH, de Castro M, Déqué M, Giorgi F, Hagemann S, Hirschi M, Jones R, Kjellström E, Lenderink G, Rockel B, Sánchez E, Schär C, Seneviratne SI, Somot S, van Ulden A, van den Hurk B (2007) An inter comparison of regional climate models for Europe: model perfor mance in present day climate. Clim Chang 81:31 52

Jacob D, Elizalde A, Haensler A, Hagemann S, Kumar P, Podzun R, Rechid D, Remedio AR, Saeed F, Sieck K, Teichmann C, Wilhelm C (2012) Assessing the transferability of the regional cli mate model REMO to different coordinated regional climate down scaling experiment (CORDEX) regions. Atmosphere 3:181 199

Jacob D et al (2001) A comprehensive model inter comparison study investigating the water budget during the BALTEX PIDCAP peri od. Meteorog Atmos Phys 77:19 43

Jacob D, Petersen J, Eggert B, Alias A, Christensen OB, Bouwer LM, Braun A, Colette A, Déqué M, Georgievski G, Georgopoulou E, Gobiet A, Menut L, Nikulin G, Haensler A, Hempelmann N, Jones C, Keuler K, Kovats S, Kröner N, Kotlarski S, Kriegsmann A, Martin E, van Meijgaard E, Moseley C, Pfeifer S, Preuschmann S, Radermacher C, Radtke K, Rechid D, Rounsevell M, Samuelsson P, Somot S, Soussana JF, Teichmann C, Valentini R, Vautard R, Weber B, Yiou P (2014) EURO CORDEX: new high resolution climate change projections for European impact research. Reg Environ Chang 14:563 578

Jacob D, Petersen J, Eggert B, Alias A, Christensen OB, Bouwer LM, Braun A, Colette A, Déqué M, Georgievski G, Georgopoulou E, Gobiet A, Menut L, Nikulin G, Haensler A, Hempelmann N, Jones C, Keuler K, Kovats S, Kröner N, Kotlarski S, Kriegsmann A, Martin E, van Meijgaard E, Moseley C, Pfeifer S, Preuschmann S, Radermacher C, Radtke K, Rechid D, Rounsevell M, Samuelsson P, Somot S, Soussana JF, Teichmann C, Valentini R, Vautard R, Weber B, Yiou P (2013) EURO CORDEX: new high resolution climate change projections for European impact research. Reg Environ Chang 14:563 578. https://doi.org/10.1007/s10113 013 0499 2

Jacob D, Podzun R (1997) Sensitivity studies with the regional climate model REMO. Meteorog Atmos Phys 63:119 129

Koldunov NV, Kumar P, Rasmussen R, Ramanathan AL, Nesje A, Engelhardt M, Tewari M, Haensler A, Jacob D (2016) Identifying climate change information needs for the Himalayan region: results from the GLACINDIA stakeholder workshop and training program. Bull Am Meteorol Soc 97:ES37 ES40

Kumar P, Podzun R, Hagemann S, Jacob D (2014) Impact of modified soil thermal characteristic on the simulated monsoon climate over South Asia. J Earth Syst Sci 123:151 160

Luca AD, Elía RD, Laprise R (2012) Potential for added value in precip itation simulated by high resolution nested regional climate models and observations. Clim Dyn 38:1229 1247

Lucas Picher P, Wulff Nielsen M, Christensen JH, Mottram R, Simonsen SB (2012) Very high resolution regional climate model simulations over Greenland: identifying added value. J Geophys Res Atmos 117:262 269

Majewski D (1991) The Europa Modell of the Deutscher Wetterdienst. In: ECMWF seminar on numerical methods in atmospheric models, pp 147 191

Prein AF et al. (2016) Precipitation in the EURO CORDEX 0.11° and 0.44° simulations: high resolution, high benefits? Clim Dyn 46:383 412

Rechid D, Hagemann S, Jacob D (2009) Sensitivity of climate models to seasonal variability of snow free land surface albedo. Theor Appl Climatol 95:197 221

Redler R (2015) YAC 1.2. 0: an extendable coupling software for earth system modelling. Geosci Model Dev

Ritter B, Geleyn J F (1992) A comprehensive radiation scheme for nu merical weather prediction models with potential applications in climate simulations. Mon Weather Rev 120:303 325

Roeckner E et al (1996) The atmospheric general circulation model ECHAM 4: model description and simulation of present day cli mate. Comptes Rendus Des Séances De La Société De Biologie Et De Ses Filiales 151:361 363

Roeckner E et al. (2003) The atmospheric general circulation model ECHAM 5. Part I: model description Report 349, Max Planck Institute for Meteorology, Hamburg

Saeed F, Hagemann S, Jacob D (2012) A framework for the evaluation of the South Asian summer monsoon in a regional climate model ap plied to REMO. Int J Climatol 32:430 440. https://doi.org/10.1002/joc.2285

Sein DV, Mikolajewicz U, Gröger M, Fast I, Cabos W, Pinto JG, Hagemann S, Semmler T, Izquierdo A, Jacob D (2015) Regionally coupled atmosphere ocean sea ice marine biogeochemistry model

ROM: 1. Description and validation. J Adv Model Earth Syst 7: 268 304

Simmons AJ, Burridge DM (1981) An energy and angular momentum conserving vertical finite difference scheme and hybrid vertical co ordinates. Mon Weather Rev 109:758 766

Taylor KE (2001) Summarizing multiple aspects of model performance in a single diagram. J Geophys Res Atmos 106:7183 7192. https://doi.org/10.1029/2000jd900719

Tiedtke M (1989) A comprehensive mass flux scheme for cumulus parame terization in large scale models. Mon Weather Rev 117:1779 1800

Wang A, Zeng X (2012) Evaluation of multireanalysis products with in situ observations over the Tibetan Plateau. J Geophys Res Atmos 117

Wang QW, Tan ZM (2014) Multi scale topographic control of southwest vortex formation in Tibetan Plateau region in an idealized simula tion. J Geophys Res Atmos 119

Wu J, Gao X (2013) A gridded daily observation dataset over China region and comparison with the other datasets. Chin J Geophys 56:1102 1111

Xu J et al (2018) On the role of horizontal resolution over the Tibetan Plateau in the REMO regional climate model. Clim Dyn:1 18

Xu Y, Gao X, Shen Y, Xu C, Shi Y, Giorgi F (2009) A daily temperature dataset over China and its application in validating a RCM simula tion. Adv Atmos Sci 26:763 772

Zhang Y, Gao H, Lammel G (2005) Simulation of monsoon seasonal variation of regional climate model REMO in East Asia (in Chinese). Climatic and Environmental Research 10:41 55

Zhou TJ, Yu RC (2005) Atmospheric water vapor transport associated with typical anomalous summer rainfall patterns in China. J Geophys Res Atmos:110